Journal Pre-proof

Buckling-enabled composite bracing for damage-avoidance rocking structures

L.T. Kibriya, C. Málaga-Chuquitaype, M.M. Kashani

PII: S0020-7403(19)31833-8
DOI: https://doi.org/10.1016/j.ijmecsci.2019.105359
Reference: MS 105359

To appear in: *International Journal of Mechanical Sciences*

Received date: 10 June 2019
Revised date: 30 September 2019
Accepted date: 6 December 2019

Please cite this article as: L.T. Kibriya, C. Málaga-Chuquitaype, M.M. Kashani, Buckling-enabled composite bracing for damage-avoidance rocking structures, *International Journal of Mechanical Sciences* (2019), doi: https://doi.org/10.1016/j.ijmecsci.2019.105359

Highlights

- The non-linear mechanics of buckling-enabled composite bracings (BECB) with circular-arc shaped cross-section are explored.
- A rigorous numerical simulation strategy for BECB elements is established and validated.
- A parametric study on the buckling behaviour of BECB members made of GFRP is performed.
- A case study of a steel rocking frame equipped with BECB is presented.
- The inclusion of BECB is successful in stabilizing the non-linear dynamic response of damageavoidance rocking frames.

Buckling-enabled composite bracing for damage-avoidance rocking structures

L.T. Kibriya[a], C. Málaga-Chuquitaype[a,*], M.M. Kashani[b]

[a] *Department of Civil and Environmental Engineering, Imperial College London, London, United Kingdom SW7 2AZ*
[b] *Faculty of Engineering and Physical Sciences, University of Southampton, Southampton, United Kingdom SO17 1BJ*

Abstract

Post-tensioned rocking frames have been proposed as damage-free seismic-resistant structures. However, currently available load resisting systems for rocking frames rely on sacrificial yielding components that accumulate damage during strong dynamic action. To address this shortcoming, this study proposes a novel thoroughly damage-avoidance solution by means of bracing elements with carefully controlled buckling behaviour. To this end, a proof-of-concept study is presented, whereby the elastic buckling response of buckling-enabled composite bracing (BECB) elements with circular-arc shaped cross-section is numerically investigated. Varying geometric properties are considered and validated against analytical approximations. Besides, a finite element study of a single-storey steel post-tensioned frame under static and dynamic actions is performed. The case study incorporates BECB elements made from glass-fibre reinforced polymer (GFRP). It is demonstrated that BECB enhances the non-linear static and dynamic response of rocking frames by providing stability and significantly reducing storey drifts and accelerations without accumulating damage.

Keywords: buckling-enabled bracing; damage-avoidance; rocking frame; non-linear dynamics; fibre reinforced polymer; finite-element

*Corresponding author
Email address: c.malaga@imperial.ac.uk (C. Málaga-Chuquitaype)

1. Introduction

In response to the severe social and economic impacts of recent earthquakes, there has been a growing interest in smart structural systems [1]. In particular, rocking self-centring frames that employ elastic gap-opening mechanisms at the column-foundation and beam-column interfaces have been proposed as damage-limiting alternatives. These systems utilise unbonded post-tensioned tendons to tie members together as well as to provide the required moment resistance and restoring forces necessary to re-centre the structure to its plumb position after strong motion. This configuration effectively prevents yielding of primary structural members, but can lead to large storey drifts and accelerations. Moreover, in order to stabilize the rocking response, sacrificial elements that dissipate modest amounts of energy through yielding (damage) are typically provided.

Research devising various methods of enhancing earthquake resilience for different classes of rocking structures has spanned over the last decade [2, 3, 4, 5, 6, 7, 8, 9, 10, 11]. In particular, in the case of self-centring frames, the use of yielding thin steel plate infill walls [12, 13, 14], buckling-restrained braces [15], yielding seat angles [16, 17], short axial yielding devices [18], yielding web hourglass pins [19], or beam web/flange friction devices [20, 21, 22] have been explored. Although these technologies are very effective in reducing peak response quantities, they all comprise of sacrificial and/or replaceable components. This results in a system with limited durability, and a requirement for frequent inspections and maintenance. Furthermore, the structures often experience permanent post-earthquake damage and require significant repair or replacement. Therefore, there is a need for alternate thoroughly damage-avoidance solutions for rocking frames.

In principle, shell elements with material properties that allow substantial global buckling while remaining largely elastic, can be employed to improve the seismic performance of self-centring rocking frames. A curvature in the cross-

section can be further introduced to increase the section's buckling capacity. A curved geometry combined with the elastic buckling motion would also provide some energy-dissipation to the structural system through sound and heat. Hence, buckling-enabled bracing, given suitable material properties, can provide stability, reduce the peak responses, and considerably improve the lateral-load resistance of self-centring rocking frames while avoiding damage.

In this context, fibre reinforced polymers (FRPs) represent an attractive material solution due to their high strength and fatigue life. FRPs are a class of composite materials made of a polymer matrix reinforced with fibres. Both GFRPs (glass-fibre reinforced polymers) and CFRPs (carbon-fibre reinforced polymers) are currently being widely researched for strengthening and retrofitting steel structures [23, 24, 25, 26, 27, 28, 29, 30, 31]. Besides its strength and fatigue-life advantages, GFRP is lightweight, durable, and non-conductive to electricity/heat [32]. Additionally, shells made of GFRP have the ability to undergo considerable elastic buckling. Therefore, they constitute an excellent material choice for the buckling-enabled composite bracing (BECB) system.

This paper investigates for the first time the use of carefully designed braces with new circular-arc cross-section in combination with rocking post-tensioned frames for the provision of truly damage-avoidance earthquake resilient structures. First, a finite element simulation strategy for the buckling members is developed and validated against analytical approximations. Next, these procedures are applied to perform a comprehensive parametric study on the buckling, post-buckling, and cyclic behaviour of GFRP elements with varying geometric properties. A significant interaction between the geometric parameters of the bracing members is identified, and their influence is shown to increase with decreasing element length. This findings are applied to the design and implementation of BECB into a prototype steel rocking frame as compression-only elements. It is demonstrated that BECB enhances the static and dynamic performance of rocking frames by significantly reducing the storey drifts and accelerations without any damage accumulation. Numerically-generated frequency response functions (FRFs) of rocking frames with and without BECB are ex-

amined and the bracing system is shown to greatly improve the stability of the rocking frame response. This proof-of-concept study forms a strong foundation towards the provision of truly damage-avoidance solutions and supplies the tools for further investigations into practical design methods.

2. Numerical Modelling of Buckling-Enabled Composite Braces

2.1. Geometric Specifications

The geometric and section properties of the BECB elements are defined in Equations 1 to 6. Figure 1 illustrates a circular arc with uniform thickness 't', outer radius 'r', chord 'c', sector angle '2α'/curvature 'α', height 'h', arc length 'l', brace length 'L', distance to the centroid from the top fibre 'y_c', and moment of inertia 'I'. In this paper, the cross-sectional geometric dimensions are defined in an orthogonal cylindrical coordinate system with an additional thickness variable (rxtxα, L).

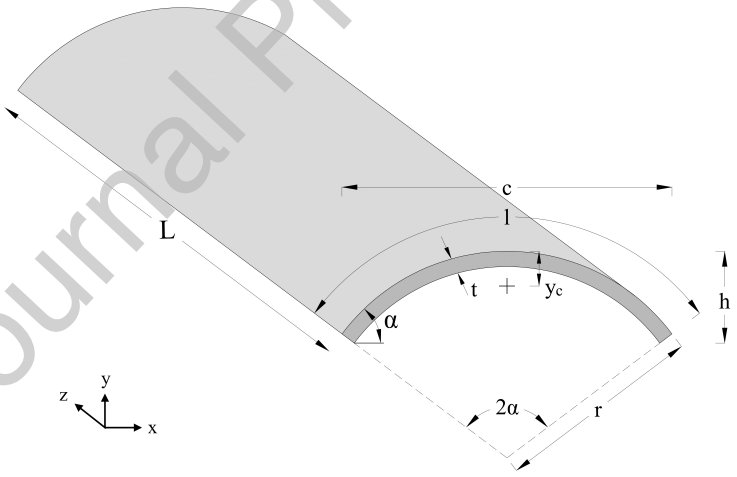

Figure 1: Geometric parameters of the bracing element

$$r = \frac{h}{2} + \frac{c^2}{8h} \tag{1}$$

$$2\alpha = 2\arcsin\left(\frac{c}{2r}\right) \tag{2}$$

$$l = 2\alpha r \tag{3}$$

$$A = \alpha(r^2 - (r-t)^2) \tag{4}$$

$$y_c = r - 2r\left(\frac{\sin(\alpha)}{3\alpha}\right)\left(1 - \left(\frac{t}{r}\right) + \left(\frac{1}{2-\frac{t}{r}}\right)\right) \tag{5}$$

$$I = \alpha t r^3\left(1 - 2\left(\frac{\sin(\alpha)}{\alpha}\right)^2 + \frac{\sin(2\alpha)}{2\alpha}\right) \tag{6}$$

2.2. Finite Element Modelling

The finite element package ABAQUS [33] was used to simulate the buckling behaviour of the BECB members. The 4-node doubly curved general-purpose shell element (designated S4R), with reduced integration and six degrees of freedom per node was selected for the models. Fixed boundary conditions were applied on one end and the other end was restrained against all movement except axial displacement (Figure 2a). Compression loads were applied to the shell by imposing uniform displacement or force along its arc length 'l', as illustrated in Figure 2b. An isotropic elastic material model with an elastic modulus 'E' of 18 GPa and Poisson's ratio 'μ' of 0.3 was used to simulate the GFRP material [34]. Four different types of analyses [35] were performed: Eigenvalue analysis, Non-linear Riks method, Static (general), and Dynamic (explicit). It is noted that the eigenvalue analysis performed does not take into account the effect of

initial imperfections and geometric non-linearity, which typically act to reduce the buckling load.

First, an eigenvalue study was performed to obtain mode shapes and linear buckling capacities (the bifurcation point). These capacities were used to validate the modelling approach adopted. The critical loads obtained from these analyses informed the subsequent non-linear analyses. The impact of varying modelling characteristics on the buckling resistances were investigated in order to form a baseline modelling methodology for the BECB. These characteristics included varying load-application techniques, meshing, and boundary conditions. The accuracy of the buckling load prediction by eigenvalue analysis was highly dependent on the mesh resolution, as expected. A mesh sensitivity study was carried out with a decreasing mesh size for elements of different geometric proportions to study the convergence in the buckling loads. The results indicated that a mesh size of two times the element thickness '2t' in both the axial and radial directions provided sufficient accuracy and stability in the results where the critical loads approached asymptotic behaviour and became relatively constant for finer meshes.

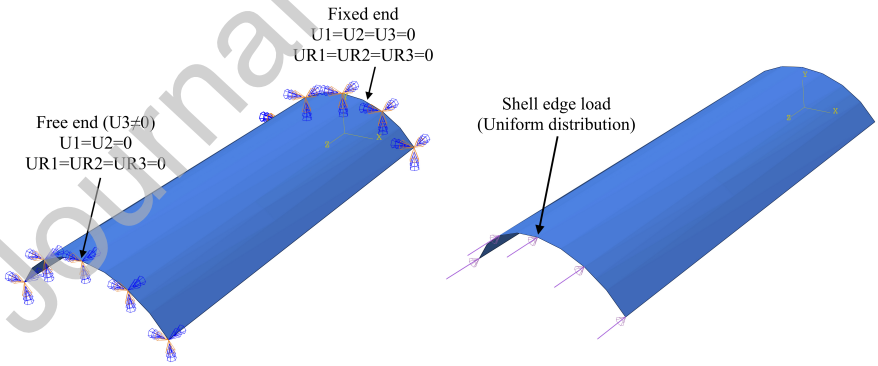

(a) Boundary conditions

(b) Load application

Figure 2: Finite element model of BECB member in ABAQUS

Similarly, the application of uniformly distributed and concentrated loads was investigated via a comparative study. The concentrated load was simulated

in two ways: firstly, by connecting the nodes along the arc length 'l' to a master node (at y_c) via rigid links, with the load applied at the master node; and secondly, by applying the point-load directly at the centre of arc length 'l'. The uniformly distributed load was multiplied by arc length 'l' to obtain equivalent concentrated loads. It was observed that these alternative load-application techniques influenced the mode shapes, in particular for aspect ratios $\frac{L}{c} < 6$. Nevertheless, for members with aspect ratios greater than 6, the buckling capacities obtained using uniform and concentrated loads were within ±2% of each other. Hence, for $\frac{L}{c} > 6$ the load application technique did not have a significant impact on the global buckling behaviour. These observations led to a baseline modelling strategy which included the load application technique, boundary conditions and mesh selection.

Following this, geometric properties for the parametric analyses were selected in accordance with reasonable archetype dimensions and practical material thicknesses. A non-linear buckling analysis was performed using the modified Riks method, which simultaneously solves for loads and displacements, mapping the response quantities in relation to the arc-length of the load-displacement curve [35, 36]. This method was utilised to study the post-buckling behaviour and carry out an imperfection sensitivity study. The linear critical load multipliers obtained from the eigenvalue analyses were applied to the shell edge (arc length 'l') at the axially free support. Axisymmetric global imperfections were introduced as scale factors for the dominant mode in both out-of-plane buckling modes. Considering the axis illustrated in Figure 1 where the cross-section is in the xy plane and the element length 'L' lies along the z axis, buckling mode A would be in the positive y direction and buckling mode B in the negative y direction. This was specified in the program by changing the sign of the imperfection multipliers.

Furthermore, the BECB members were subjected to uniaxial loading and un-loading compression cycles using displacement control, in the static (general) and dynamic (explicit) analyses. A general static analysis was performed using consecutive loading/unloading steps (for example Step 1: 0-50mm, Step

2: 50-0mm). The cyclic axial displacements were applied using the amplitude versus time input available. Lateral displacements were recorded at the point of maximum out-of-plane deflection (buckle). It is noted that initial global imperfections were necessary for convergence and hence included in the general static and dynamic analyses. The buckling capacities and post-buckling behaviour obtained from the general static and Riks analyses were used to provide an indicator for the cyclic buckling .

Subsequently, buckling was investigated using a dynamic (explicit) analysis to simulate slow compression tests allowing for the investigation of the associated force-displacement response. ABAQUS performs dynamic analysis, using a Lagrangian formulation and integrating the equations of motion in time explicitly by means of central differences [33]. An implicit integration operator was also utilised to evaluate critical buckling loads, however, the results from both operators were nearly identical, and the explicit scheme was selected for the remaining investigations to reduce processing time. Moreover, the displacements were applied in a quasi-static manner.

3. Model Validation

The results obtained from eigenvalue analyses were compared with the critical buckling loads estimated through the analytical model developed in [37] for deployable structures which has been itself experimentally validated. The purpose of this was to validate the numerical modelling strategy developed for buckling-enabled braces in the preceding section. In particular, equations 7 and 8 were used to estimate the critical buckling loads, for a range of element lengths [37].

$$\sigma_{\mathrm{cr}} = 0.6\frac{Et}{r} \tag{7}$$

$$\sigma_{\mathrm{cr}} = P_{\mathrm{cr}}\left(\frac{1}{A} + \frac{e^2}{Icos\sqrt{\frac{P_{\mathrm{cr}}L^2}{4EI}}}\right) \tag{8}$$

where σ_{cr} is the critical stress for a cylindrical panel under compressive load and e is the eccentricity or the distance from the neutral axis (y_c). The remaining variables have been previously defined in Section 2.

Steel material properties, as presented in [37], were applied for both models with an elastic modulus 'E' of 210 GPa. The cross-sectional dimensions used were 19 mm x 0.1 mm x 0.65 rad (rxtxα). Two point-loads were applied on each end at the center of arc length 'l', and all degrees of freedoms were restrained except axial displacement at both ends. This method of load application was adopted directly from [37]. It is important to note that buckling-enabled bracing is not limited to the use of GFRP. Conceptually, any material which permits the required elastic buckling behaviour can be employed to achieve similar results, hence the choice of material properties mentioned above.

The analytical and numerical results are compared in Figure 3. The critical buckling loads are calculated using equation 9

$$\lambda = \frac{PL^2}{EI} \tag{9}$$

and the lengths were normalized using the chord c $\left(\frac{L}{c}\right)$. All dimensional quantities are presented in millimetres and radians in Figure 3. It is evident from this figure that the results from both analyses are in good agreement, with the numerical values being approximately 3% higher than the analytical predictions. Hence, the numerical modelling protocol presented herein was demonstrated to be reliable for investigating the behaviour of shell BECB elements. Following validation, these numerical procedures were further applied to perform an in-depth parametric study in the following sections.

4. Buckling, Post-buckling and Cyclic Response

4.1. Buckling Response

A detailed parametric study was devised in order to achieve a complete understanding of the influence of geometric design parameters on the overall

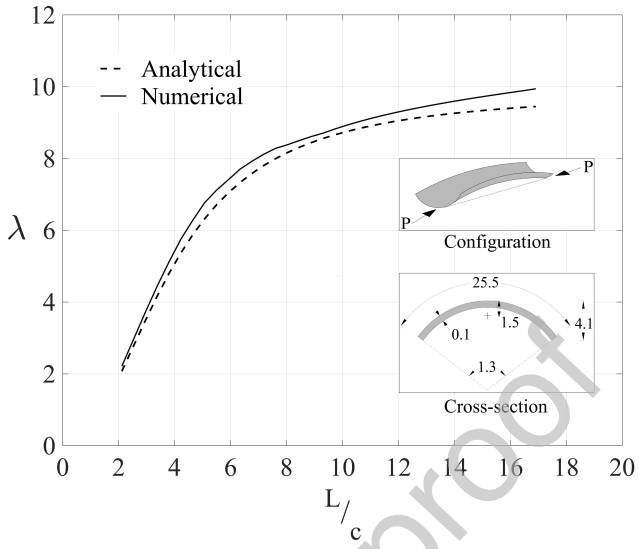

Figure 3: Comparison of the buckling behaviour of buckling elements represented using numerical and analytical predictions

buckling behaviour of BECB. The insights gained from this process will facilitate the design of BECB sections for implementation in steel rocking frames presented later in this paper.

The first three buckling modes for a GFRP element with $\alpha = 50°$, $\frac{L}{c} = 10$, and $\frac{t}{r} = 20\%$ are presented in Figure 4. These were obtained using an eigenvalue analysis, as detailed in Section 2. The material experiences axisymmetric out-of-plane buckling when subjected to uniform in-plane compression, with axial waves increasing in number for higher modes, as expected. It can be observed that the modal shapes achieved using the aforementioned geometric proportions are similar to the typical buckling modes of a flat rectangular plate, as discussed further below.

The mode shapes were notably dependent on the thickness and curvature of the elements. Members with $\frac{L}{c} < 10$, $\frac{t}{r} < 10\%$, or $\alpha < 40°$ exhibited in-plane deformation as their primary eigen-mode. For members with $\frac{L}{c} < 3$, the out-of-plane buckling mode (Figure 4a) was between the 4-7th modes. Moreover,

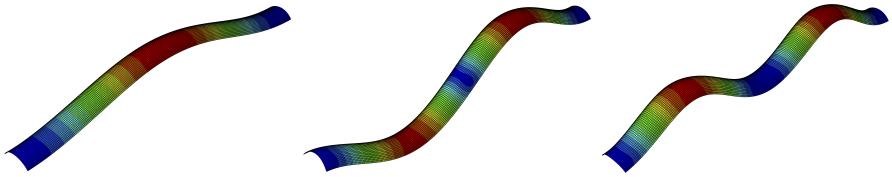

(a) First mode (b) Second mode (c) Third mode

Figure 4: Modal shapes for a GFRP element with $\frac{L}{c} = 10$, $\alpha = 50°$, and $\frac{t}{r} = 20\%$

members with increasing curvature and decreasing thickness experienced higher levels of in-plane deformations, or local buckling in the circumferential plane. It was also noted that elements with $\frac{L}{c} < 10$ and $\frac{t}{r} < 10\%$ did not exhibit axially symmetric buckling, and the maximum point of deflection was observed at approximately 0.6L-0.7L from the fixed end, rather than at 0.5L. In contrast, the curvature did not have a major impact on the buckling symmetry. This implies that for the previously mentioned proportional limits of $\frac{L}{c} > 10$, $\frac{t}{r} > 10\%$, or $\alpha > 40°$ (e.g. Figure 4), the member behaves similar to a flat rectangular plate with roller-fixed end boundary conditions. Consequently, the linear buckling loads were compared to values estimated through the analytical formulations presented in Section 3. Compared with the analytical predictions, maximum differences of less than 5% in the critical load magnitudes were obtained. These conclusions were further applied to formulate an in-depth parametric study for the BECB members.

4.2. Imperfection Sensitivity and Post-Buckling Response

Imperfection sensitivity analysis can be used to provide an indication of the stability behaviour of an element. An imperfection sensitivity analysis was first performed on elements of varying lengths and constant thicknesses 't' and curvatures 'α'. The imperfection effects were characterized by means of the knockdown factor [38], obtained by dividing the buckling load of the imperfect system (P) by the buckling load of the perfect system (P_{max}). Figure 5 illustrates knockdown curves with the knockdown factors ($\frac{P_{max}}{P}$) plotted against the out-of-plane displacement ($\Delta_{lateral}$) expressed as a percentage of the member

length (L). Similarly, the magnitude of imperfections is presented as a multiple of the relevant member thickness. The imperfection behaviour of the elements was evaluated for two possible bucking modes for an element with $\frac{L}{c} = 12$, $\alpha = 40°$, and $\frac{t}{r} = 10\%$.

It can be noted from Figure 5 that the element appears to be sensitive to large imperfections, with a 20% reduction in the critical buckling load 'P_{cr}' with every 't' increase in the imperfection amplitude. Nevertheless, this sensitivity is reduced for imperfections of the order of 't' to '3t' and markedly minor for magnitudes lower than 't'. A 5% decrease in the buckling capacity with each 0.2t increase in the imperfection magnitude was observed. Comparing Figures 5a and 5b, it can be observed that buckling mode A exhibits a drop in the buckling strength at $\frac{\Delta_{lateral}}{L} = 7\%$. This was due to the snap-transition of the top curved fibre to a flat section, with increasing applied force. Similarly, a small instantaneous drop was observed at $\frac{\Delta_{lateral}}{L} = 15\%$ for buckling mode B. However, it is noted that mode B follows a more stable deformation path, exhibiting a gradual reduction in the buckling resistance as the out-of-plane deflection increases. Moreover, the buckling resistances for buckling mode B were found to be 2% higher than those recorded for mode A. Following these observations, and considering the advantages of GFRP manufacturing, imperfections that facilitate mode B buckling were applied for all analyses presented in the remainder of this article. It was concluded that initial imperfections with amplitudes less than 't' did not have a remarkable effect on the buckling capacity of the BECB elements.

4.3. Parametric Study of Buckling Behaviour

Figures 6 to 8 illustrate the results of the parametric study. The geometric properties were systematically changed, and their effect on the buckling response of BECB was studied. Figure 6 presents the buckling resistance for variable values of thickness 't', plotted for a range of aspect ratios ($\frac{L}{c}$) and constant curvature 'α'. Figure 7 illustrates the buckling resistance with variable curvature 'α', presented for a range of aspect ratios ($\frac{L}{c}$) and constant thickness parameter

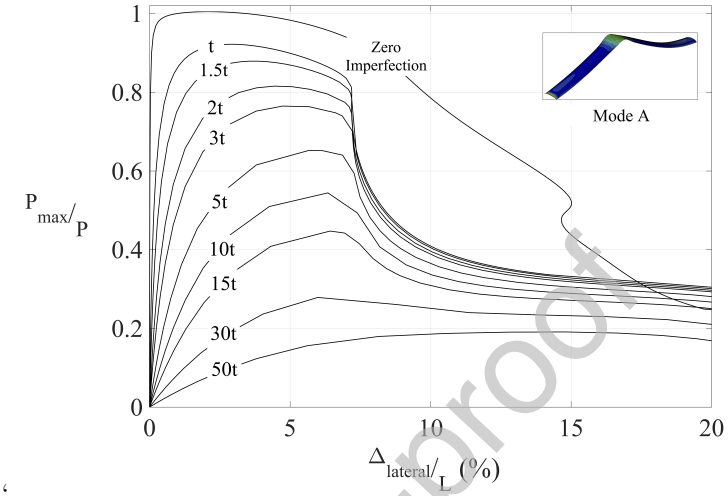

(a) Buckling mode A

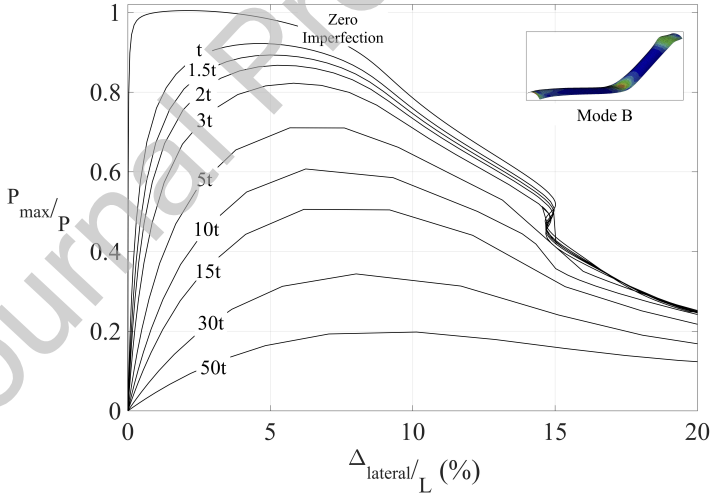

(b) Buckling mode B

Figure 5: Imperfection sensitivity analysis for different buckling modes for a GFRP element with $\frac{L}{c} = 12$, $\alpha = 40°$, and $\frac{t}{r} = 10\%$

't'. Figure 8 presents the buckling resistances for variable values of thickness 't', plotted for a range of thickness-to-radius ratios ($\frac{t}{r}$) and constant length parameter 'L'.

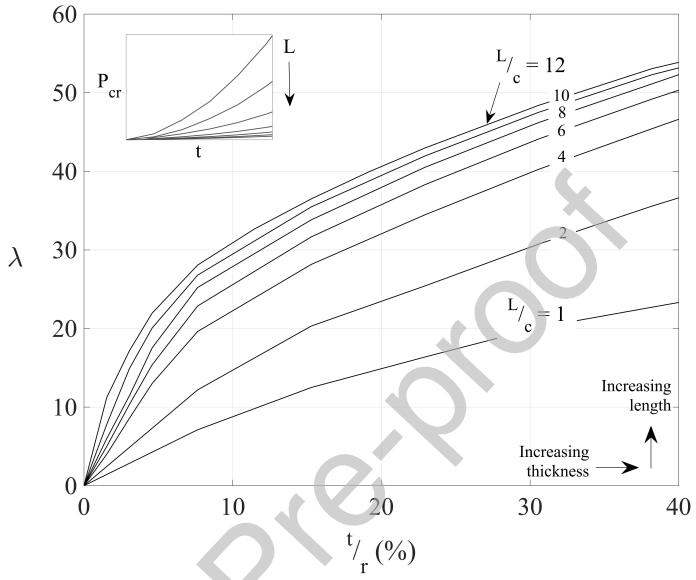

Figure 6: Relationship between the buckling resistance and thickness for GFRP BECB elements of varying lengths and constant curvature

A clear increase in buckling resistance 'P_{cr}' with increasing member thickness 't' for a constant curvature 'α' is apparent from Figure 6. Moreover, the change in curvature 'α' has a greater impact on elements with lower aspect ratios ($\frac{L}{c}$). Hence, it is evidenced that there is a strong interaction between the aspect ratio ($\frac{L}{c}$) and thickness 't' parameters. For $\frac{L}{c} \leq 5$, it is observed that every 1 mm increase in thickness leads to a 25% higher buckling resistance. For $\frac{L}{c} > 5$, the corresponding buckling resistance is 40% higher for every 1 mm thickness 't' increment. The changing slope of the buckling curves at $\frac{t}{r} = 7\%$ indicates that the moment of inertia 'I' increases more rapidly with increasing thickness 't' than the corresponding critical buckling loads 'P_{cr}'. This leads to a change in the slope of the buckling curve. These observations provide a fundamental

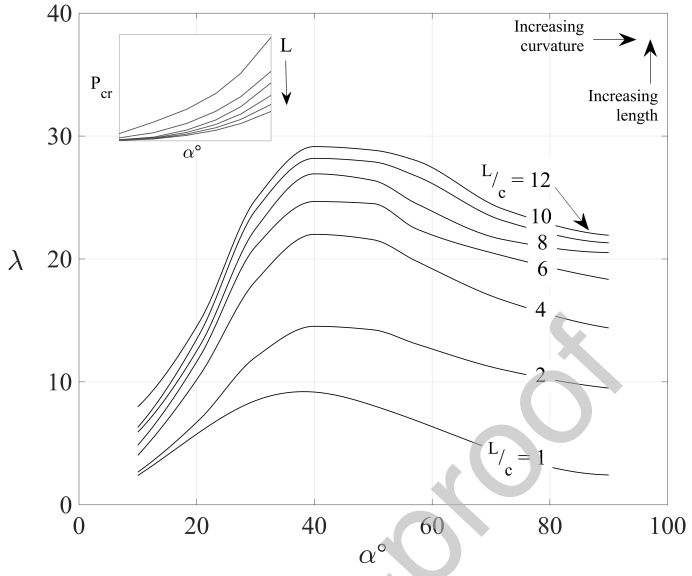

Figure 7: Relationship between the buckling resistance and curvature for GFRP BECB elements of varying lengths and constant thickness

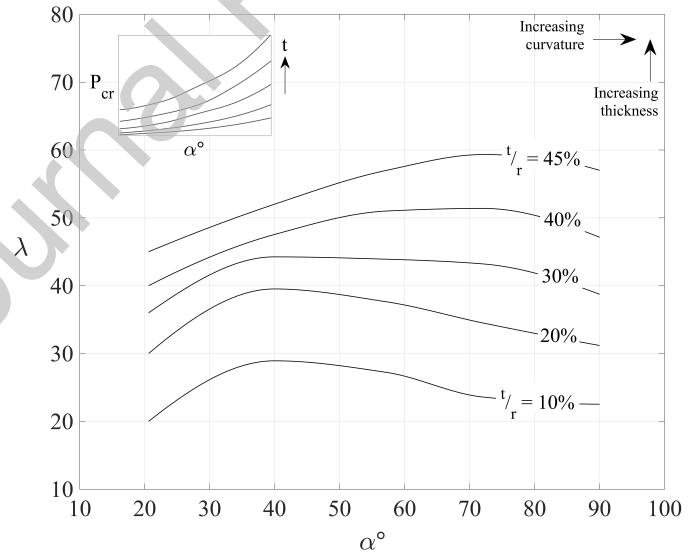

Figure 8: Relationship between the buckling resistance and curvature for GFRP BECB elements of varying thickness and constant length

guideline for selecting optimal design thickness 't' of BECB elements.

Figure 7 demonstrates that the buckling load factor 'λ' increases with increasing curvature 'α', given constant thickness 't', until maximum values are reached at $\alpha = 40°$. This trend is followed by a declining buckling curve. Additionally, for $\alpha > 60°$, the GFRP BECB member exhibited large in-plane deflections and significant local buckling. The negative slope occurs due to the rapidly ascending magnitudes of moment of inertia 'I' whose rate of increase is relatively higher than the increase in the buckling strength 'P_{cr}', which results in a negative slope in the buckling curve. In dimensional terms, every +6° curvature increment resulted in an approximately 25% greater critical buckling load 'P_{cr}'. This response is usually observed when flat rectangular plates are morphed into a curved cross-section, which leads to an increase in the moment of inertia and hence the buckling resistance. Following these observations, the curvature of a specific element can be selected, with the optimal angle found to be between 30° to 60° for the majority of cases. Similar to the interaction between the thickness 't' and aspect ratio '$\frac{L}{c}$', the curvature 'α' was found to be more effective in increasing the buckling strength for elements with lower aspect ratios.

In consideration of the complex interaction between the curvature 'α' and aspect ratios '$\frac{L}{c}$', the variation of curvature 'α' was further evaluated in combination with variable thickness 't' and constant length 'L'. To this end, Figure 8 shows that the resulting buckling curves follow a curved path. It is noted that the '$\frac{t}{r}$' ratio changes with each curvature amplitude and therefore the curves are labelled using the '$\frac{t}{r}$' ratios for the maximum possible curvature for each element (at α=90°). In contrast to the previous figures, the transition between '$\frac{t}{r}$' ratios is constant, with a reduction in the critical buckling load of 30% for each 10% decrease in thickness 't'.

The previously presented figures are also reproduced as surfaces tin Figure 9 to provide a more integral appreciation of the interaction between different parameters along a broader data range. To this end, the surfaces were estimated using a cubic interpolation function in MATLAB and the goodness-of-fit

parameters were verified using the curve fitting toolbox [39]. It is evident from Figure 9 that the curvature of the cross-section 'α' is particularly effective in altering the fundamental mode shapes of the BECB elements, whereas the thickness 't' significantly impacts their buckling strength. It should be emphasized that this cross-section has not been studied in this context previously. Hence, it is important to examine the influential geometric characteristics in order to design an effective structural system. A design guideline can therefore be established in order to select suitable geometric proportions for BECB members for application in damage-avoidance rocking frames. The first step would be to determine the section length and the required buckling strength of the element. Next, a chord dimension should be selected. It is recommended to select a $\frac{L}{c}$ ratio between 8-10 as an initial design configuration as the buckling capacities tend to stabilize for these ratios. Another advantage of these proposed ratios is to start with a minimized material requirement (Higher $\frac{L}{c}$ means a narrower cross-section, given a constant L). Figures 6 or 9a would then be used to determine the required member thickness. Consequently, a combination of these parameters can be employed to select a curvature α using the data presented in Figures 7 and 8, or 9b and 9c. This method was followed to design the bracing elements for the steel rocking frame presented in the subsequent sections.

4.4. Unloading Response

Figure 10 compares buckling curves obtained using both linear and nonlinear analysis options available in ABAQUS [33]. An imperfection amplitude equal to the element thickness 't' was considered in the static and dynamic analyses. Different types of analyses (Riks, static and dynamic) were performed to trace the loading-unloading paths under cyclic uni-axial compression. The numerical predictions of the buckling strengths experienced differences of less than 2% between the Riks method (with imperfections), Static and Dynamic analyses. Also, the critical loads P_{cr}' obtained from the eigenvalue analyses and Riks method (without imperfections) are virtually identical.

During unloading, the BECB member follows the shortest linear distance

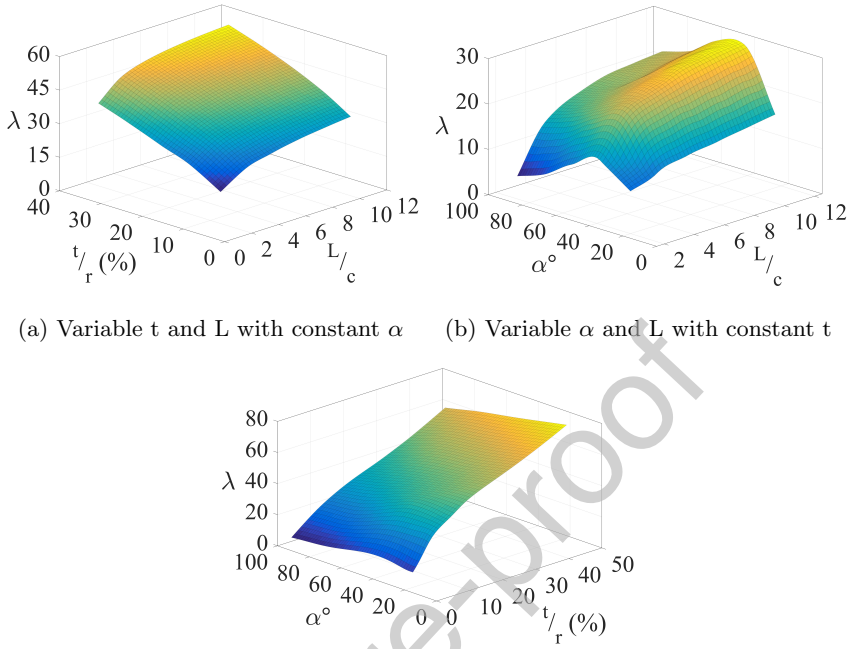

(a) Variable t and L with constant α

(b) Variable α and L with constant t

(c) Variable α and t with constant L

Figure 9: Surfaces formed by combining the data presented in Figures 6 to 8 using cubic interpolation

to return to its original plumb position. Hence, all deformations were fully recovered. This is a key behavioural characteristic of the type of cross-section examined in this paper and one that plays a crucial role in the damage-avoidance applications explored herein. For smaller displacements, prior to reaching the critical buckling load 'P_{cr}', the loading and unloading slopes were equal. After 'P_{cr}', the element experiences a snap-back motion during unloading. The member is unstable at the point of unloading and deforms instantaneously back to its initial stable state. In cases where the element is unloaded gradually, the snap-back occurs along the shortest path to reach each increment of the applied displacement. This means that for infinitesimal unloading increments, the path can be inferred to follow the original loading slope. It is highlighted that buckling of the bracing elements will provide some energy-dissipation due

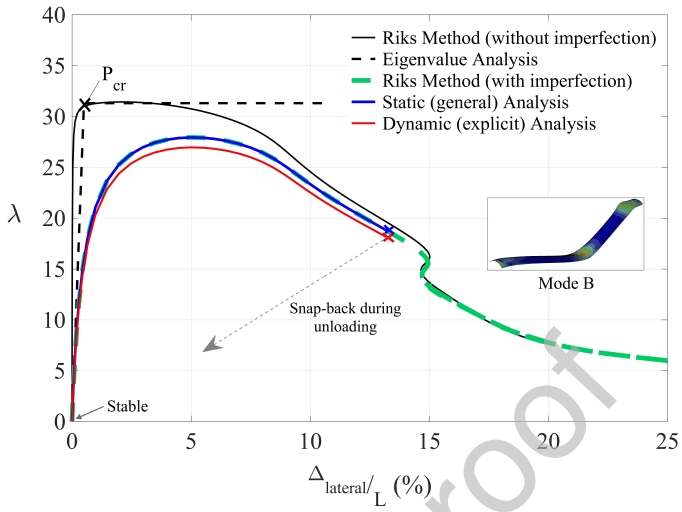

Figure 10: Buckling behaviour obtained using various solution methods in the finite element program ABAQUS

to the generation of heat and sound. Nevertheless, this is extremely difficult to quantify using conventional FE tools. Therefore, the material is assumed to exhibit negligible energy-dissipation in the following stages of this investigation. It is also worth noting that the BECB elements do not exhibit any plastic behaviour. Since the buckling of the members is bi-stable elastic, it is expected that the system will not accumulate damage. This allows us to proceed with the application of BECB to steel rocking frames.

5. Application of BECB to Steel Rocking Frames

5.1. Proposed Structures

The structural model employed as a case study is a one-storey full-scale single-bay planar steel frame, comprising of moment-resisting rocking connections at the beam-to-column and column-to-foundation interfaces. Figure 11 presents a schematic of the proposed frame. The frame has a storey height of 3.5 m and bay width of 5 m. These values correspond to an aspect ratio of 0.8. The floor beam was designed at a centreline of 0.35 m from the base. RHS

section 250 x 150 x 16 (mm) are selected for the floor beam, and RHS 350 x 250 x 16 (mm) for the remaining beam and column elements. A tendon cross section of 150 mm^2 is incorporated. S275 steel with an elastic modulus of 210 GPa is employed for the steel members. The applied mass on the frame is 15 tonnes. This frame is representative of the rocking behaviour of self-centring structures and is consistent with prototypical models previously employed to explore the fundamental non-linear dynamics of rocking frames [40]. The interested reader is referred to [40] for a comprehensive validation of the numerical model against experiments.

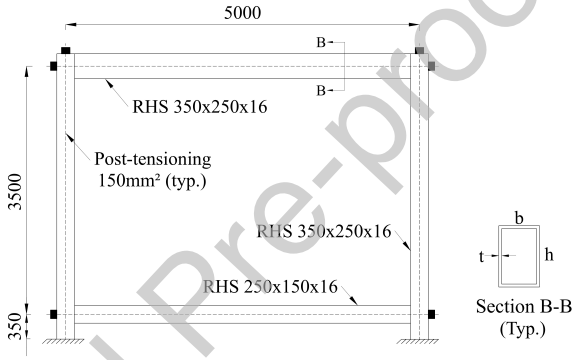

Figure 11: One-storey, single bay steel rocking frame

The proposed configurations for the BECB are presented in Figure 12. For configuration 1, two sizes of BECB (8 elements in total) are incorporated, including shorter members with dimensions of L = 1.9 m, $\alpha = 50°$, t = 6 mm, r = 100 mm and longer members with L = 3.8 m, $\alpha = 49°$, t = 7 mm, r = 180 mm. For configuration 2, BECB elements (4 in total) are incorporated, with dimensions of L = 1.9 m, $\alpha = 46°$, t = 15 mm, r = 200 mm.

5.2. Finite Element Modelling and Analysis Parameters

The finite element programme OpenSEES (Open System for Earthquake Engineering Simulation, [41]), was utilised for all numerical analyses. The rocking frame was simulated using the numerical modelling procedures for both static

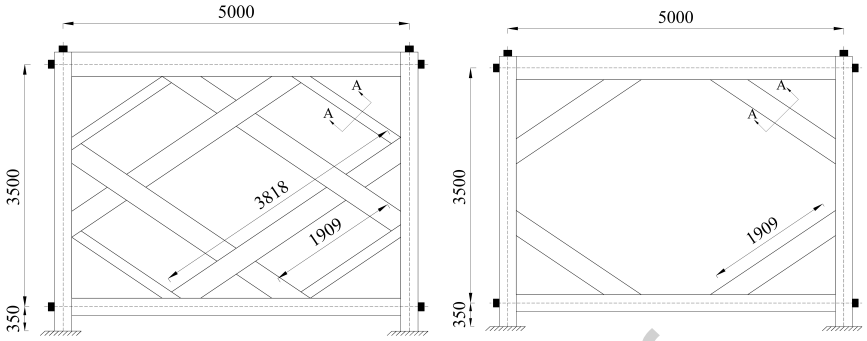

(a) Configuration 1 (b) Configuration 2

Figure 12: Configurations of GFRP bracing elements incorporated into a steel rocking frame

and dynamic analyses proposed in [40]. Planar frames with three-degrees-of-freedom per node were defined. All degrees of freedom were constrained at the foundation level to simulate a fixed base beneath the rocking interface. Nodal masses were defined in the horizontal and vertical degrees of freedom, and lumped at the top of each column element.

The columns and tendons were modelled as continuous elements along the frame height. The post-tensioning tendons were modelled using *Corotational Truss Elements* with an initial stress uniaxial material (*Steel02* material in OpenSees [41]). S275 steel with an elastic modulus of 210 GPa was used for the beam and column members. Elastic beam-column elements were used for modelling the beams and columns since plastic deformations are not expected in these members. *Zero-length* gap elements (springs) were used to simulate the rocking surfaces. Elastic Perfectly Plastic material with no tension stiffness was defined for the gap element. The Lobatto integration scheme introduced in [42], was used to determine the distribution of the gap elements along member edges.

Figure 13 illustrates the application of the Elastic Perfectly Plastic uniaxial material used to represent the pre to post-buckling behaviour of BECB. The material properties were callibrated to the buckling response obtained from

ABAQUS [33]. The critical load (λ_{cr}) represents the point of transition from an unbuckled state to a buckled state. Subsequently, the bracing members were represented as truss compression-only elements in the frame models. Beam gravity loads were applied as nodal loads on the columns. The static lateral loads were also applied at the nodes assuming linear first-mode distribution. A displacement control strategy was used to perform the non-linear static analysis.

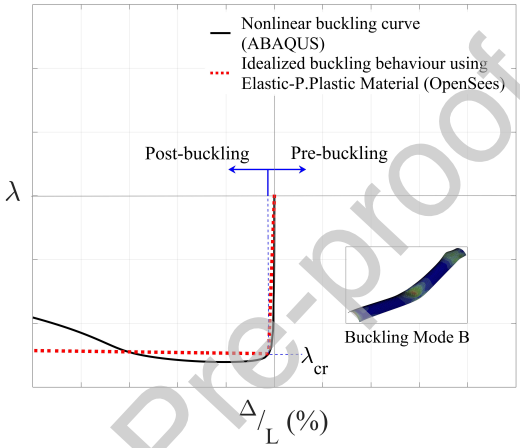

Figure 13: OpenSEES material model calibrated to ABAQUS buckling curve

Frequency response functions (FRFs) were selected to evaluate the benefits of applying BECB to rocking steel frames since they provide insight into the complex and unconventional dynamic behaviour of non-linear structural systems [40, 43]. Although they are regularly obtained from numerical searches of periodic stable solutions along the spectrum [43], in the present case FRFs were generated using discrete sine-sweep input ground motions as originally proposed in [40]. To this end, the frequency was incremented by discrete amounts, giving the structure time to reach a steady-state response. MATLAB [39] was used to generate input harmonic base motions. The response-history obtained from the discrete sine-sweep analyses comprised of a transient and a steady-state dynamic response. The steady-state response for each excitation frequency increment was isolated and the time was converted to the frequency domain, to

generate the FRFs.

6. Structural Response of Steel Rocking Frames Equipped with BECB

6.1. Static Analysis and Monotonic Response

The results of the static analysis for the two configurations of the single-storey frame under consideration, are illustrated in Figure 14. This figure plots the base shear 'V' against roof drift ($\frac{\Delta}{H}$). The base shear 'V' was normalised using the total weight of the frame 'W'.

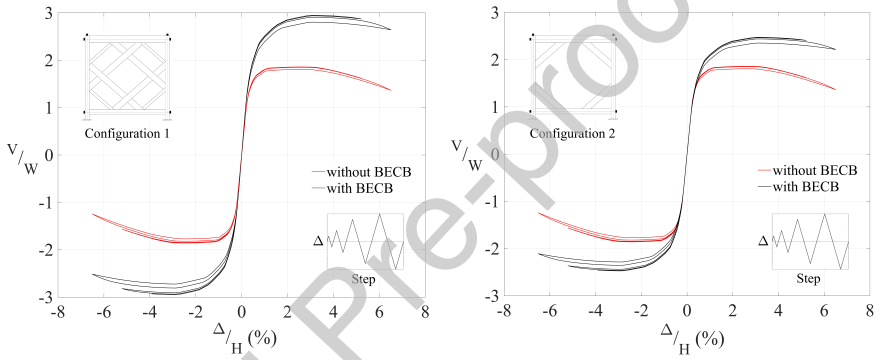

(a) Configuration 1 (b) Configuration 2

Figure 14: Comparison of static responses of steel rocking frames with and without GFRP bracing elements

Each frame configuration was subjected to a series of four horizontal cycles. The resulting data is presented in Figure 14 comparing the roof drifts of the rocking frame with and without BECB. The figures demonstrate that the bracing elements significantly increase the lateral load carrying capacity of both structural configurations. Frame configuration 1 exhibits a 30% increase in the lateral load resistance whereas configuration 2 shows a 15% increase. Additionally, Figure 14 demonstrates that the frames experiences zero residual drifts and damage accumulation.

6.2. Dynamic Analysis and Frequency Response Functions (FRFs)

A series of dynamic analyses were performed for low, medium, and high forcing amplitudes. FRFs were formulated using the methods described in section 5.2, and are presented in Figures 15 and 16. The frequencies are normalised against the natural frequencies of the corresponding finite element models. The FRFs are plotted in terms of roof drifts and accelerations since these response parameters are widely used as indicators of structural and non-structural damage [44, 45]. By plotting the FRFs for a range of forcing amplitudes, a backbone curve is constructed. Moreover, the FRFs were utilised to identify the fundamental frequencies of the building models using the maximum inflection points of the low-amplitude curves. It is noted that the rocking joints do not open during the low-amplitude FRFs (0.005g), and the frame behaves linearly. For these low-amplitude FRFs, the inclusion of BECB did not have a significant impact on the response quantities, as expected.

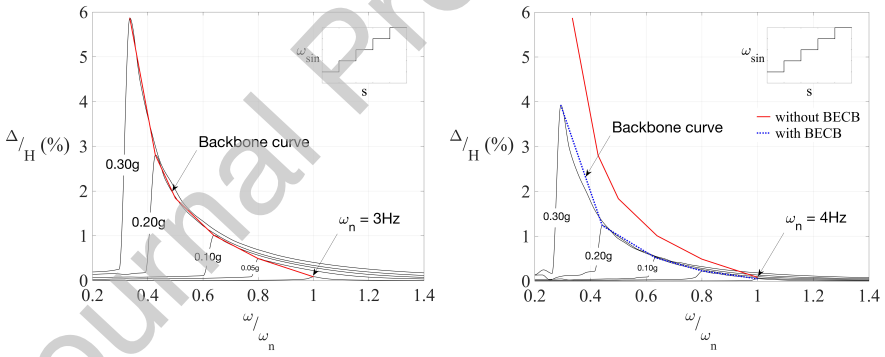

(a) Rocking Frame without BECB (b) Rocking Frame with BECB

Figure 15: Comparison of frequency response functions (FRFs) storey drifts responses for steel rocking frames with and without Buckling-Enabled Composite Bracing

It can be observed from Figures 15 and 16 that the natural frequency of the frame with BECB is approximately 4Hz and the frame without BECB has a natural frequency of 3Hz. Therefore, it is apparent that the buckling-enabled braced frame is stiffer than its pure rocking frame counterpart. More impor-

tantly, Figure 15 demonstrates that for all excitation levels (0.005g-0.30g), the inclusion of BECB members reduces the roof drifts by upto 40%. In the case of frame configuration 2, the drifts experience a reduction of upto 25%. Figure 16 further compares the roof accelerations of both systems. It is evident that the roof accelerations for medium and high amplitude excitations (0.20g-0.30g) show a substantial reduction of upto 50% due to the introduction of BECB. Similarly, the accelerations obtained using low amplitude excitation (0.005g-0.10g) experience a 15% reduction. Likewise, for frame configuration 2, the BECB rocking frame system resulted in 35% lower magnitudes under medium to high amplitude excitations (0.20g-0.30g). The decrease in the accelerations for frame configuration 2 was determined to be 10% for low excitation amplitudes (0.005g-0.10g).

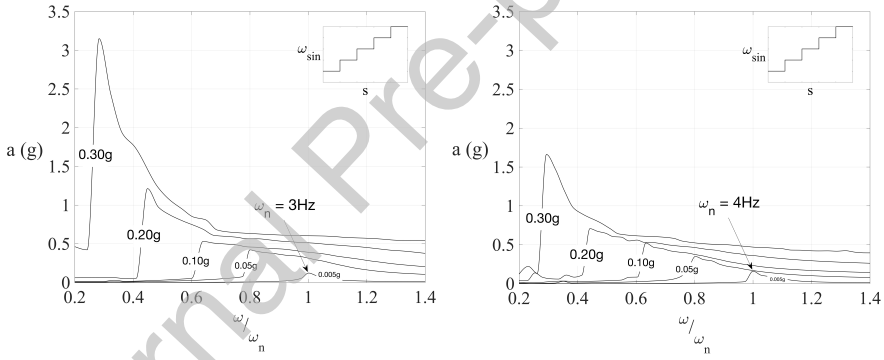

(a) Rocking Frame without BECB (b) Rocking Frame with BECB

Figure 16: Comparison of frequency response functions (FRFs) roof acceleration responses for steel rocking frames with and without Buckling-Enabled Composite Bracing

From the foregoing it is evident that steel rocking frames equipped with BECB result in significantly lower peak response quantities. Besides, BECB was also observed to enhance the overall stability of the rocking structure. The time for the rocking frame to reach steady-state (processing time) during each frequency step, decreased by 40% with the addition of BECB. Numerical convergence during the analyses was also achieved significantly quicker. Interestingly,

for high amplitude excitations, both structures (with and without BECB) experienced sub-harmonic frequencies occurring at a lower than resonant frequency. The rocking frames with BECB exhibited these sub-harmonics very close to (almost overlapping) the resonant frequencies (Figure 16). In contrast, the rocking frames without BECB exhibited more prominent sub-harmonics at 1/2 resonant frequency of the particular excitation amplitude. This indicates that the implementation of BECB also reduces the dynamic non-linearities in the rocking frame while providing outstanding stability.

6.3. Practical Considerations

The newly proposed BECB system relies on the controlled elastic buckling of GFRP members that do not accumulate plastic strains. Therefore, it is crucial that a compression-only response is ensured. Figure 17 proposes a connection between the BECB and the steel members. This connection was designed to prevent tensile strains in the BECB while ensuring a robust compression-only behaviour. The curved BECB members are first bolted to steel blocks. The edges of the block are then bolted to an angle, which in turn is welded to the column. The brace end of the angle is provided with slotted bolt holes parallel to the BECB axis in order to permit the frames movement while the beam-to-BECB interface is fixed. During the lateral movement of the frame, the fixed beam-end of the brace moves in the direction of the frame. This causes the free column-end of the brace on one side to move diagonally upwards because of the angled slots. This motion in turn relieves any axial forces in the brace and prevents tension. Meanwhile, the corresponding brace in the opposite direction remains at the bottom of the slot. The detail presented in Figure 17 allows a transfer of compressive forces during lateral movement, causing the brace to buckle, but prevents tension stresses to be developed in the BECB

Another practical consideration is that the proposed system is expected to remain elastic for typical recurrent lateral loads such as winds. The BECB members can be tuned to allow activation of the buckling response leading to a change in the dynamic behaviour only during periods of high demand. It is further em-

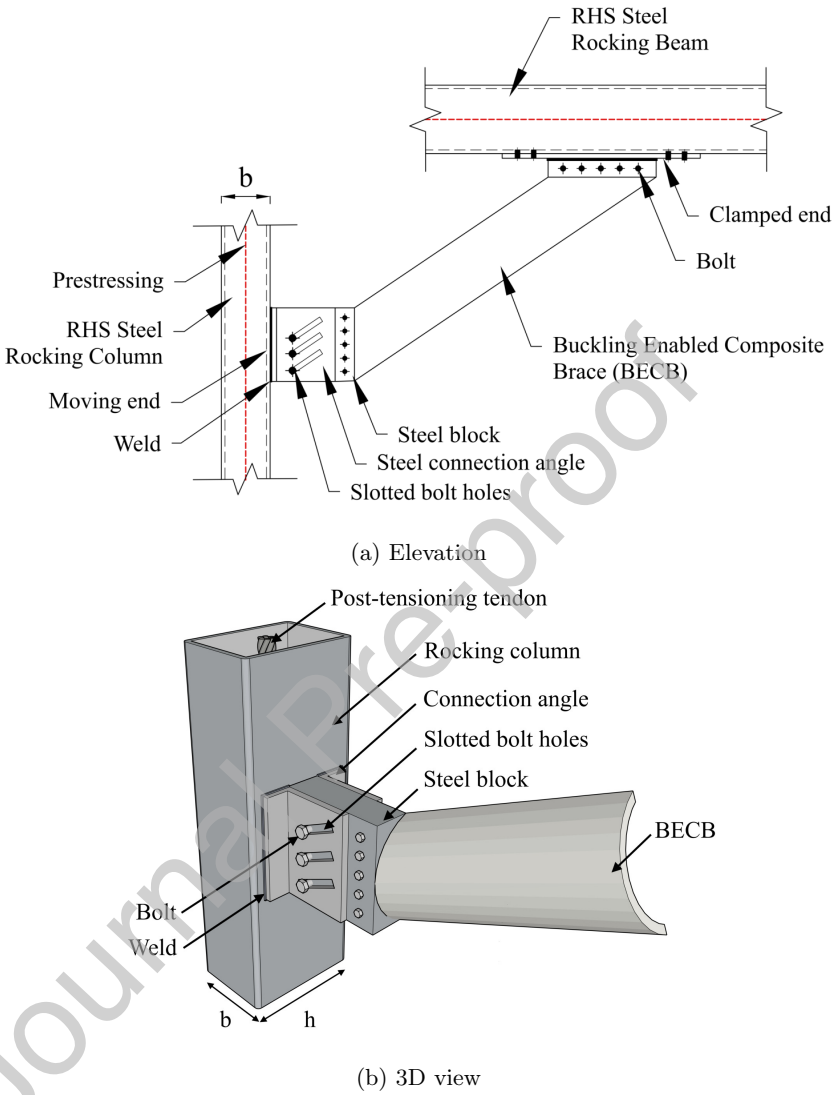

Figure 17: Proposed connection detail for BECB to steel frame

phasized that this paper introduces a new cross-section and material application. It presents the proof-of-concept by applying the BECB to steel rocking frames and comparing the resulting behaviour. It is clear that the proposed BECB system significantly improves the performance of steel rocking frames under lateral

loads. Moreover, energy-dissipation of the system can be improved by exploring different assemblies and cross-sections of GFRP or the use of other composite materials [46] if required. The findings presented herein will allow future investigations dedicated to the advancement of this proposal, including life-cycle cost assessment and numerical testing under earthquake ground motions.

7. Conclusions

Currently available lateral-load resisting systems for rocking frames comprise of replaceable yielding components that are damaged after strong motion leading to non-negligible maintenance costs and downtime. By applying the recoverable elastic buckling properties of the newly proposed bracing elements with circular-arc shaped cross-section this paper has demonstrated that a thoroughly damage-avoidance rocking system can be realized. First, a numerical simulation strategy was established for the BECB and validated using analytical approximations. Next, the procedures were applied to perform an extensive parametric study on the buckling behaviour of BECB elements made of GFRP for different combinations of geometric parameters. Finally, the knowledge gained through these analyses was applied to design and implement BECB into a prototype steel rocking frame. The main research findings of this study are summarized below.

Non-linear mechanics of BECB

- The buckling modes of the BECB elements with circular-arc shaped cross-section resemble those of a typical flat rectangular plate, however, members with $\frac{L}{c} < 10$, $\frac{t}{r} < 10\%$, or $\alpha < 40^\circ$ exhibited severe in-plane deformation.

- For imperfections lower than a thickness amplitude t, the BECB is less sensitive to imperfections, with a 5% decrease in the buckling capacity for each 0.2t increase in the imperfection amplitude.

- For aspect ratios of $\frac{L}{c} \leq 5$, every +1 mm increase in thickness leads to a 25% higher buckling resistance. This value increases to 40% for aspect ratios $\frac{L}{c} > 5$.
- Every 6° curvature 'α' increment results in an approximately 25% higher critical buckling load 'P_{cr}'.
- A reduction in critical buckling loads 'P_{cr}' of 30% are obtained for each 10% decrease in the thickness 't'.
- The values of the critical buckling loads 'P_{cr}' obtained using the Eigenvalue, Riks, Static, and Dynamic analyses were within a maximum of ±3% of each other.
- The curvature 'α' of the BECB sections is particularly effective in changing their fundamental mode shapes, whereas the thickness 't' can significantly increase their buckling strengths.

Non-linear mechanics of rocking frames equipped with BECB

- The structural system with 8 BECB members exhibited a 30% increase in the lateral load resistance compared to the frame without BECB.
- The frame with 4 short BECB elements designed with a larger curvature and thickness, exhibited a 15% increase in the buckling resistance.
- A 40% reduction in drifts was observed in the rocking frame with BECB when subjected to harmonic sweep motions.
- A 50% reduction in roof accelerations was observed in the braced steel rocking frame, for medium to high amplitude excitations.
- For low amplitude excitations, a 15% reduction in accelerations was observed due to the inclusion of BECB.
- The inclusion of BECB reduced the time required to reach steady-state response by 40% and stabilized the full non-linear dynamic response.

- The rocking frames with BECB exhibited less prominent sub-harmonics that were closer to the resonant frequency of the FRF than the frames without BECB.

Overall, it has been demonstrated that the proposed damage-avoidance structural system can significantly improve the non-linear dynamic response of self-centring rocking frames. Moreover, important insight has been gained into the buckling and post-buckling response of elements with circular-arc shaped cross-section, a configuration that has not been explored in preceding literature. The findings and tools developed herein constitute an important step towards the provision of truly damage-avoidance structures.

AUTHOR DECLARATION OF NO CONFLICT OF INTEREST

SUBMIT2IJMS_2019_1790

Buckling-enabled composite bracing for damage-avoidance rocking structures by Leena Kibriya and Dr Christian Mlaga-Chuquitaype (corresponding author) and Dr Mohammad Kashani. We wish to confirm that there are no known conflicts of interest associated with this publication and there has been no significant financial support for this work that could have influenced its outcome. We confirm that the manuscript has been read and approved by all named authors and that there are no other persons who satisfied the criteria for authorship but are not listed. We further confirm that the order of authors listed in the manuscript has been approved by all of us. We confirm that we have given due consideration to the protection of intellectual property associated with this work and that there are no impediments to publication, including the timing of publication, with respect to intellectual property. In so doing we confirm that we have followed the regulations of our institutions concerning intellectual property. We understand that the Corresponding Author is the sole contact for the Editorial process (including Editorial Manager and direct communications with the office). He is responsible for communicating with the other authors about progress, submissions of revisions and final approval of proofs. We confirm

that we have provided a current, correct email address which is accessible by the Corresponding Author and which has been configured to accept email from Elsevier. Signed by Dr Christian Mlaga-Chuquitaye (Corresponding Author) on behalf of all authors:

References

[1] D. Kellenberg, A. Mobarak, The Economics of Natural Disasters, Annual Review of Resource Economics 3 (1) (2011) 297–312.

[2] M. Priestley, S. Sritharan, J. Conley, S. Pampanin, Preliminary Results and Conclusions From the PRESSS Five-Story Precast Concrete Test Building, PCI Journal 44 (6) (1999) 42–67.

[3] Y. C. Kurama, R. Sause, S. Pessiki, L.-w. Lu, Seismic Response Evaluation of Unbonded Post-Tensioned Precast Walls, ACI Structural Journal (99-S66) (2002) 641–651.

[4] B. G. Morgen, Y. C. Kurama, A Friction Damper for Post-Tensioned Precast Concrete Moment Frames, PCI Journal (3189) (2004) 112 – 133.

[5] M. R. Eatherton, J. Hajjar, G. G. Deierlein, H. Krawinkler, S. Billington, X. Ma, Controlled rocking of steel-framed buildings with replaceable energy-dissipating fuses, Proceedings of the 14th World Conference on Earthquake Engineering (2008) 12–17.

[6] D. Roke, R. Sause, J. Ricles, N. Gonner, Design Concepts for Damage-Free Seismic-Resistant Self-Centering Steel Concentrically Braced Frames, ASCE Structures Congress Austin, Texas, USA.

[7] M. R. Eatherton, J. Hajjar, X. Ma, H. Krawinkler, G. Deierlein, Seismic design and behavior of steel frames with controlled rocking: part I-concepts and quasi-static subassembly testing, ASCE Structures Congress (1) (2010) 1534–1543.

[8] X. Ma, Seismic Design and Behavior of Self-Centering Braced Frame with Controlled Rocking and EnergyDissipating Fuses, Phd thesis, Stanford University (2010).

[9] T. L. Karavasilis, S. Kerawala, E. Hale, Hysteretic model for steel energy dissipation devices and evaluation of a minimal-damage seismic design approach for steel buildings, Journal of Constructional Steel Research 70 (2012) 358 – 367.

[10] L. L. Song, T. Guo, Y. Gu, Z. L. Cao, Experimental study of a self-centering prestressed concrete frame subassembly, Engineering Structures 88 (2015) 176–188.

[11] R. Thiers-Moggia, C. Málaga-Chuquitaype, Seismic protection of rocking structures with inerters, Earthquake Engineering & Structural Dynamics 48 (5) (2019) 528–547.

[12] P. Timler, C. E. Ventura, H. Prion, R. Anjam, Experimental and analytical studies of steel plate shear walls as applied to the design of tall buildings, The Structural Design of Tall Buildings 7 (3) (1998) 233–249.

[13] P. M. Clayton, J. W. Berman, L. N. Lowes, Subassembly testing and modeling of self-centering steel plate shear walls, Engineering Structures 56 (2013) 1848–1857.

[14] D. M. Dowden, R. Purba, M. Bruneau, Behavior of self-centering steel plate shear walls and design considerations, Journal of Structural Engineering 138 (January) (2011) 11–21.

[15] L. Wiebe, Design of Controlled Rocking Steel Frames to Limit Higher Mode Effects, PhD Thesis Department of Civil and Environmental Engineering, University of Toronto, Canada.

[16] J. Ricles, R. Sause, M. Garlock, C. Zhao, Posttensioned Seismic-Resistant Connections for Steel Frames, Journal of Structural Engineering 127 (2) (2001) 113–121.

[17] R. Sause, J. M. Ricles, M. M. Garlock, E. Vanmarcke, L.-s. Peh, J. Liu, B. Shear, Self-Centering Seismic-Resistant Steel Frame Systems : Overview of Past and Current, Precast Concrete 2–4.

[18] C. Christopoulos, A. Filiatrault, C.-M. Uang, B. Folz, Posttensioned Energy Dissipating Connections for Moment-Resisting Steel Frames, Journal of Structural Engineering 128 (9) (2002) 1111–1120.

[19] G. Vasdravellis, B. Uy, T. L. Karavasilis, Experimental validation of steel post-tensioned connections with web hourglass pins, Stessa 2012: Proceedings of the 7th International Conference on Behaviour of Steel Structures in Seismic Areas 139 (June) (2012) 677–683.

[20] J. Iyama, C.-y. Seo, J. M. Ricles, R. Sause, Self centering MRFs with bottom flange friction devices under earthquake loading, Journal of Constructional Steel Research 65 (2) (2008) 314–325.

[21] H.-J. Kim, C. Christopoulos, Friction Damped Posttensioned Self-Centering Steel Moment-Resisting Frames, Journal of Structural Engineering 134 (11) (2008) 1768–1779.

[22] Y.-C. Lin, J. M. Ricles, R. Sause, C.-y. Seo, Earthquake Simulations on a Self-Centering Steel Moment Resisting Frame with Web Friction Devices, Structures Congress 2009 (2009) 1–10.

[23] S. Moy, ICE Design and Practice Guide : FRP composites Life extension and strengthening of metallic structures, Thomas Telford.

[24] L. C. Hollaway, J. Cadei, Progress in the technique of upgrading metallic structures with advanced polymer composites, Progress in Structural Engineering and Materials 4 (2) (2002) 131–148.

[25] M. Tavakkolizadeh, H. Saadatmanesh, Fatigue Strength of Steel Girders Strengthened with Carbon Fiber Reinforced Polymer Patch, Journal of Structural Engineering 129 (2) (2003) 186–196.

[26] S. C. Jones, S. A. Civjan, Application of Fiber Reinforced Polymer Overlays to Extend Steel Fatigue Life, Journal of Composites for Construction, ASCE 7 (4) (2003) 331–338.

[27] K. Nozaka, C. K. Shield, J. F. Hajjar, Effective Bond Length of Carbon-Fiber-Reinforced Polymer Strips Bonded to Fatigued Steel Bridge I-Girders, Journal of Bridge Engineering 10 (2) (2005) 195–205.

[28] N. J. Lombardi, J. Liu, Glass fiber-reinforced polymer/steel hybrid honeycomb sandwich concept for bridge deck applications (2011).

[29] K. Deng, P. Pan, X. Nie, X. Xu, P. Feng, L. Ye, Study of GFRP Steel Buckling Restraint Braces, Journal of Composites for Construction 19 (6) (2015) 04015009.

[30] M. F. Sá, L. Guerreiro, A. M. Gomes, J. R. Correia, N. Silvestre, Dynamic behaviour of a GFRP-steel hybrid pedestrian bridge in serviceability conditions. Part 1: Experimental study, Thin-Walled Structures 117 (February) (2017) 332–342.

[31] F. Zhang, W. Liu, Z. Ling, H. Fang, D. Jin, Mechanical performance of GFRP-profiled steel sheeting composite sandwich beams in four-point bending, Composite Structures 206 (August) (2018) 921–932.

[32] A. S. Mosallam, Composites: Construction Materials for the New Era, Advanced Polymer Composites for Structural Applications in Construction (2004) 45–58.

[33] M. Smith, ABAQUS/Standard User's Manual, Version 6.9, Simulia, 2009.

[34] T. Sathishkumar, S. Satheeshkumar, J. Naveen, Glass fiber-reinforced polymer composites–a review, Journal of Reinforced Plastics and Composites 33 (13) (2014) 1258–1275.

[35] R. Paulo, P. Carlone, R. Valente, F. Teixeira-Dias, F. Rubino, Numerical simulation of the buckling behaviour of stiffened panels: Benchmarks for

assessment of distinct modelling strategies, International Journal of Mechanical Sciences 157 (2019) 439–445.

[36] M. A. Crisfield, A fast incremental/iterative solution procedure that handles snap-through, in: Computational Methods in Nonlinear Structural and Solid Mechanics, Elsevier, 1981, pp. 55–62.

[37] S. Pellegrino, C. Green, S. Guest, A. A. Watt, SAR Advanced Deployable Structure, Cued/D-Struct/Tr191 (19673).

[38] H. Wagner, C. Hühne, Robust knockdown factors for the design of cylindrical shells under axial compression: potentials, practical application and reliability analysis, International Journal of Mechanical Sciences 135 (2018) 410–430.

[39] I. MathWorks, Matlab: The language of technical computing, MATLAB Primer Massachusetts, United States of America.

[40] L. Kibriya, C. Málaga-Chuquitaype, M. Kashani, N. Alexander, Nonlinear dynamics of self-centring rocking steel frames using finite element models, Soil Dynamics and Earthquake Engineering 115 (2018) 826–837.

[41] F. McKenna, Object-oriented finite element programming: Frameworks for analysis, algorithms and parallel computing, PhD Thesis Department of Civil and Environmental Engineering, University of California Berkeley, United States of America.

[42] H. Spieth, A. Carr, A. Murahidy, D. Arnolds, M. Davies, J. Mander, Modelling of post-tensioned precast reinforced concrete frame structures with rocking beam-column connections, New Zealand Society of Earthquake Engineering 2004 Conference Canterbury, New Zealand.

[43] C. Málaga-Chuquitaype, C. Menendez-Vicente, R. Thiers-Moggia, Experimental and numerical assessment of the seismic response of steel structures with clutched inerters, Soil Dynamics and Earthquake Engineering 121 (2019) (2019) 200–211.

[44] C. Málaga-Chuquitaype, Estimation of peak displacements in steel structures through dimensional analysis and the efficiency of alternative ground-motion time and length scales, Engineering Structures 101 (2015) 264–278.

[45] C. Málaga-Chuquitaype, M. Psaltakis, G. Kampas, J. Wu, Dimensionless fragility analysis of seismic acceleration demands through low-order building models, Bulletin of Earthquake Engineering 1–31.

[46] M. Kashani, E. Ahmadi, A. Gonzalez-Buelga, D. Zhang, F. Scarpa, Layered composite entangled wire materials blocks as pre-tensioned vertebral rocking columns, Composite Structures 214 (2019) (2019) 153–163.